Soil Arching in Geosynthetic-Reinforced Pile-supported Railway Embankments under the Seismic Condition

Naveen Kumar Meena[1], Sanjay Nimbalkar[2,*]

1. Ph.D. student, School of Civil and Environmental Engineering, University of Technology Sydney, Broadway NSW 2007, Australia. Email: Naveenkumar.Meena@student.uts.edu.au

2. Senior Lecturer, School of Civil and Environmental Engineering, University of Technology Sydney, Broadway NSW 2007, Australia. Email: Sanjay.Nimbalkar@uts.edu.au *(Corresponding author)

Abstract

The geosynthetic-reinforced pile-supported (GRPS) embankments provide feasible solutions for railway infrastructure projects on the soft soil due to rapid construction and less differential settlements. In the GRPS embankments, soil arching plays a crucial role in transfer of loads from soft soil to pile. However, seismic investigation of the soil arching is yet to be fully known. Therefore, this study is focused on the seismic investigation of soil arching in a GRPS railway embankment using two-dimensional (2D) finite element modelling. Results demonstrate that the seismic excitation significantly affects the soil arching. Therefore, the transient nature of soil arching should be considered in the design to ensure the GRPS embankment stability in earthquake-prone regions. It is also evident that the inclusion of reinforcement can improve the load transfer mechanism by membrane effect and further reduce the load on subsoil.

Keywords: Pile, Embankment, Geosynthetics, Earthquake, Soil arching, Finite elements

1 Introduction

The geosynthetic-reinforced pile-supported (GRPS) embankments provide feasible solutions for construction of railroad on the soft soil due to rapid construction and less differential settlements. In the GRPS embankments, soil arching is a key mechanism for load transfer from subsoil to pile top. Several finite element method (FEM) based numerical studies (Han and Gabr 2002; Huang et al. 2009; Nunez et al. 2013; Meena et al. 2020), and model tests (Chen et al. 2010; Iglesia et al. 2014; Fagundes et al. 2017; Rui et al. 2019) have been conducted to investigate the soil arching under the static loading condition.

The dynamic behaviour of soil arching is also investigated under cyclic loading, representing traffic loading, in few recent studies (Han et al. 2015; Niu et al. 2018; Pham and Dias 2019). Han et al. (2015) conducted a series of model tests and the FEM based numerical simulations and it is found that the reinforcement and subsoil characteristics can enhance soil arching mobilisation under the dynamic loading. Niu et al. (2018) reported that the height of soil arching is reduced under the dynamic load induced by high-speed train compared to the static loading condition. Pham and Dias (2019) investigated the behaviour of a GRPS embankment subjected to cyclic loading. However, the seismic analysis of soil arching is yet to be investigated for GRPS embankments.

Although, Australia is widely recognised as a seismically non-active country, small to moderate seismic activities continue to occur (Daniell and Love 2010). The locations of these seismic events in Australia are illustrated in Figure 1. This study is aimed to perform such analysis for GRPS embankments.

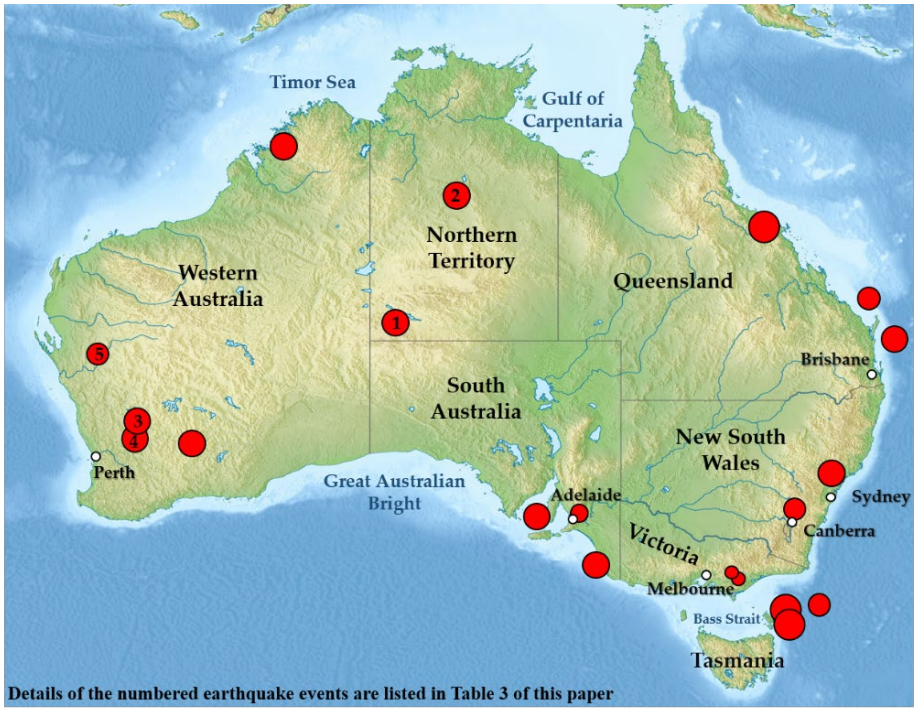

Figure 1. Locations of the key seismic events in Australia (map adopted from Geoscience Australia)

2 Numerical Modelling

In this study, finite element modelling (FEM) is employed using software ABAQUS 2018. The soil arching phenomenon is assessed under seismic excitation in two-dimensional (2D) plane-strain condition. The 2D modelling is widely used to reduce computational time and the facility for analysis (Huang and Han 2010; Wu et al. 2019). The geometric profile and details of FE

model such as constitutive model, material properties, boundary condition, and element type are explained herein. In addition, the analysis procedure is also mentioned.

2.1 *Geometric Profile of FE Model*

A portion of a typical GRPS embankment as illustrated in Figure 2 is considered for numerical simulation. The geometric profile of the finite element (FE) model consisting of 8 m subsoil underlain by the hard stratum is considered. The end bearing piles, with 1 m in diameter (D_{Pile}) and 8 m in length, are chosen for this study. The pile spacing (s) is considered 2.5 m. An embankment fill including a 400 mm thick reinforced gravel layer is laid over the piled foundation. A 2 mm thick geosynthetic layer is sandwiched in between two layers of the gravel bed. First, a 200 mm thick gravel layer is placed on the piled improved subsoil area then the layer of geosynthetic is laid without any physical damage. Another 200 mm thick gravel layer is placed on the geosynthetic top in order to the achieve required thickness of gravel layer (i.e., 400 mm). The embankment height (h) is considered 3.5 m. Subsequently, an equivalent dynamic load induced by a moving train speed of 40 km/h is considered on the embankment top. The equivalent dynamic load is equal to the weight of the train multiplied by dynamic amplification factor (DAF), which accounts for the dynamic effects due to the moving train (Doyle NF. 1980; Esveld, C. 2001).

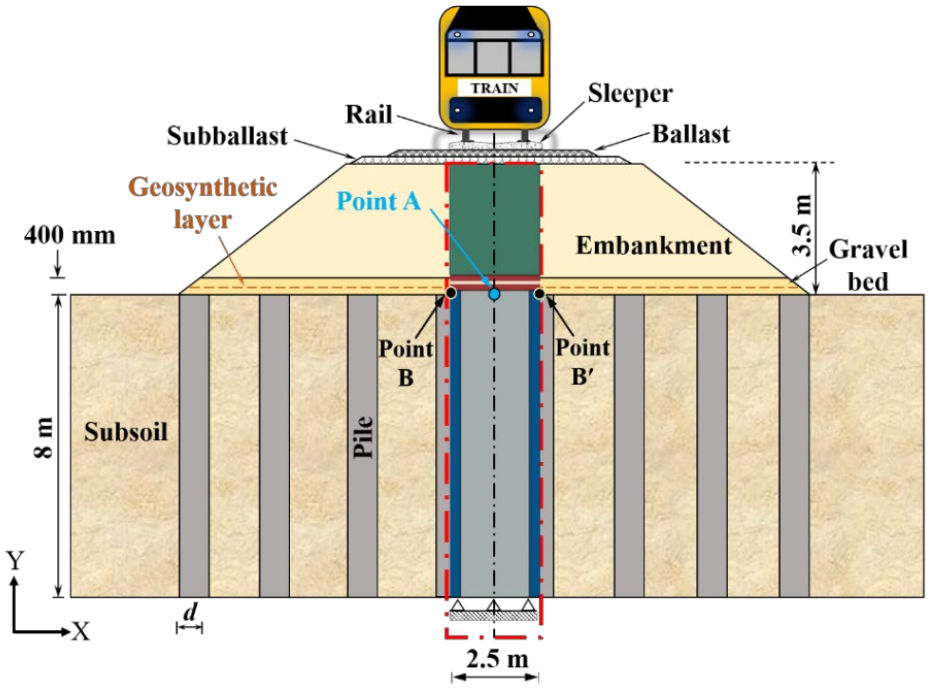

Figure 2. A typical GRPS embankment with analysed region

Fundamentally, the GRPS embankment is a three-dimensional (3D) problem and it requires high computational time and extensive resources for the analysis. In the contrast, a 2D numerical analysis can conveniently be adopted. It is recognised that the predictions of 3D and 2D conditions can differ if an appropriate conversion method is not used. In the past, various conversion methods were reported for convert 3D GRPS embankment into 2D. It was found that the Equivalent Area (EA) method is in good agreement with the 3D model (Zhang et al. 2014; Wu et al. 2019). Therefore, EA method is adopted in this study to convert FE model to 2D for further analysis.

2.2 FE Modelling Details

2.2.1 Constitutive Model and Material Properties

The Mohr-Coulomb (MC) constitutive model is chosen for embankment fill and gravel layers. The subsoil is modelled as modified cam clay (MCC). The piles and geosynthetic layer are assumed to follow an isotropic linear elasticity. The Young's modulus of pile (E_p) and geosynthetic layer are considered as 20 GPa and 500 MPa, respectively. The biaxial geogrid containing the rib thickness of 2 mm is used as geosynthetic layer. Table 1 illustrates the material properties used in this study.

Table 1. Material properties used in this study (Liu et al. 2007; Meena et al. 2020)

Material properties	Embankment fill	Gravel bed	Subsoil	Geosynthetic layer (2 % tensile strain)
Constitutive model	MC	MC	MCC	Linear elastic
Unit weight, γ (kN/m^3)	20	21	18.4	-
Young's modulus, E (MPa)	20	25	-	500
Poisson's ratio, v	0.25	0.25	0.30	0.30
Effective cohesion c′ (kPa)	0.1	0.1	-	-
Effective friction angle, ϕ' (degree)	30	35	-	-
Effective dilation angle, ψ (degree)	0	5	-	-
Critical-state stress ratio, M	-	-	1.2	-
Logarithmic hardening constant, λ	-	-	0.06	-
Logarithmic bulk modulus, k	-	-	0.012	-
Initial yield surface size, a_o (kPa)	-	-	103	-
Void ratio at unit pressure, e_1	-	-	0.87	-
Initial void ratio, e_o	-	-	0.45	-
Geosynthetic stiffness, J (kN/m) = $E \times t$	-	-	-	1000

2.2.2 Rayleigh Damping

In the seismic analysis, energy dissipation occurs which is referred to hysteretic damping. This damping can significantly influence the FE model response. Rayleigh damping instead of viscous damping is used in the FE analysis to get a correct response of the FE model during seismic analysis. The Rayleigh damping is obtained as (Nimbalkar et al. 2012):

$$[C] = \alpha[M] + \beta[K'] \quad (1)$$

where, [C] is damping matrix, [M] is mass matrix, [K'] is stiffness matrix, α and β are the damping coefficients calculated as:

$$\alpha = 2 \times \left(\frac{\omega_i.\omega_j}{\omega_i+\omega_j}\right) \times \xi_0 \quad (2)$$

$$\beta = \left(\frac{2}{\omega_i+\omega_j}\right) \times \xi_0 \quad (3)$$

where, α and β are the Rayleigh damping coefficients which can be obtained using first two vibration modes i and j, respectively; ω_i and ω_j are the angular frequencies of the vibrating material, and ξ_o is damping ratio. The damping ratio (ξ_o) is assumed as 3% to compute the damping coefficients α and β. Material response in seismic analysis depends on its dynamic characteristics. Therefore, it is crucial to determine the Rayleigh damping coefficients

precisely. Table 2 shows the dynamic parameters used in the FE model to compute the Rayleigh damping coefficients.

Table 2. Dynamic parameters used in the present study

Material type	Stiffness coefficient, *k* (10^8) (N/m)	Damping coefficient, *c* (10^6) (Ns/m)	Angular frequencies (rad/s)		Rayleigh damping coefficient	
			ω_i	ω_j	α	β
Embankment fill	0.03	0.21	31.74	158.68	1.5868	0.0003
Gravel bed	0.30	0.24	268.36	1341.76	13.4178	0.00004
Subsoil	0.01	0.14	8.89	44.45	0.4445	0.0011

2.2.3 Boundary Condition and Element Type

The base of the numerical model is fully fixed, while the vertical boundaries are laterally restrained. The base and lateral boundaries are extended to longer dimensions to avoid wave refection from the FE model and get accurate results. The Lateral boundaries is extended to 25D while base is extended to 5D. The eight-node plane strain element with reduced integration (CPE8R) is used for FE Model. The basic coulomb friction model is used to simulate the pile-subsoil interaction (Potyondy, J. G. 1961).

2.2.4 Interface modelling

The pile-soil interaction is simulated using the basic Coulomb friction model (Meena et al. 2021). This interaction is introduced using surface to surface contact. The normal contact is provided as “hard contact”, while the tangential contact is considered as penalty contact with a friction coefficient of 0.7 at the pile-soil interface.

2.3 Seismic Input

The horizontal acceleration time history of the Christchurch 2011 earthquake is considered. A few Australian earthquakes follow similar seismic parameters with Christchurch 2011 earthquake (Meena and Nimbalkar 2019). Therefore, the acceleration time history of this earthquake is chosen for this study. The magnitude of this Earthquake was 6.3 M_L on the Richter scale with 0.34g peak ground acceleration (PGA) for 30 s. Table 3 lists details of some of key Australian earthquakes. The earthquake simulated in this study has parameters similar to these earthquakes reported in Table 3 while Figure 1 shows the locations of these earthquakes in Australia.

Table 3. Details of few Australian earthquakes (data sourced from Geoscience Australia)

Year	Australian territory/state	Earthquake magnitude (M_L)	Peak ground acceleration (PGA)
2016	Northern Territory	6.1	0.49g
1988	Northern Territory	6.6	0.30g
1979	Western Australia	6.1	0.20g
1968	Western Australia	6.5	0.20g
1941	Western Australia	6.3	0.20g

2.4 *FE Simulation Procedure*

The numerical analysis starts with establishing initial stress in subsoil using the geostatic step. Installation of rigid piles and stage construction of the GRPS embankment including gravel bed and geosynthetic layer are simulated in the following steps. After attaining full embankment height, an equivalent dynamic load is imposed on the embankment top. Subsequently, in the earthquake condition, the horizontal acceleration time history of the Christchurch 2011 earthquake is applied at the base of FE model. For simplicity, the fully drained condition is assumed.

3 Results and Discussion

In the GRPS embankment, mobilisation of soil arching can be assessed with regard to vertical stress variation above on point A (referred to Figure 2). The vertical stress distribution in an unreinforced embankment on point A is considered as a reference case for a better understanding of soil arching which is shown in Figure 3 with dash-dotted line. It is evident that the vertical stress gradually increases and follows geostatic stress from the embankment top to 2.3 m embankment height. This embankment height represents the outer boundary of soil arching. The vertical stress trend decreases below the outer boundary of soil arching up to 0.6 m embankment height. This embankment height is denoted as the inner boundary of soil arching. In this region located between the outer - inner boundaries of soil arching, the majority of vertical stress is transferred to the pile top. However, a slight increase in vertical stress can be observed due to the self-weight of soil beneath the inner boundary of soil arching. In contrast for the earthquake condition, the vertical stress is linearly increased from the embankment top to base under the unreinforced state. It implies that the soil arching is not mobilised under seismic excitation. As shown in Figure 3, reinforcement can help in development of the soil arching under the earthquake condition. It is shown that the vertical stress initially increases from the embankment top to 1.9 m embankment height which represents the outer boundary of soil arching. Further, it decreases up to 0.5 embankment height, denoting the inner arch. It is also evident that the vertical stress at the embankment base is lower compared to unreinforced state for the seismic case. In contrast, the vertical stress significantly increases at the embankment base compared to the static condition. It thus implies that geosynthetic reinforcement enhances the soil arching mobilisation in the pile-supported embankment in static and seismic cases.

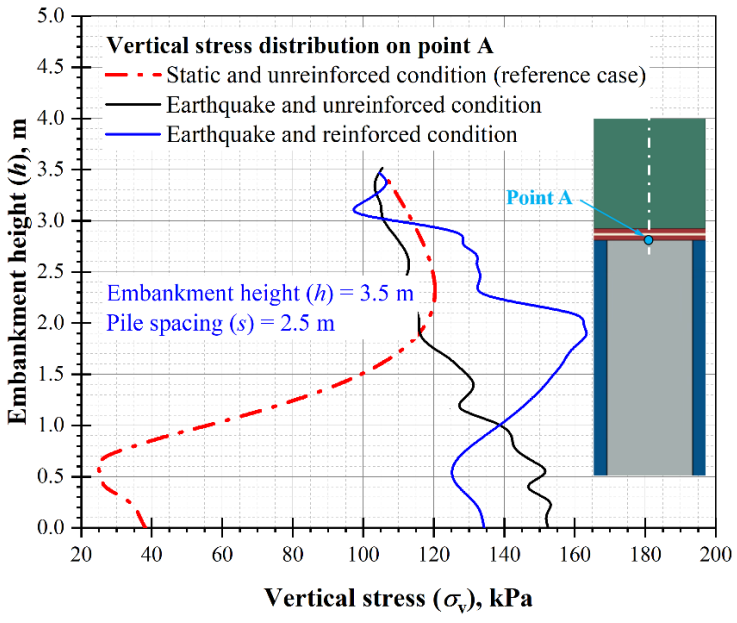

Figure 3. Vertical stress above point A in embankment under different scenarios

Figure 4 shows the variation in soil arching ratio (SAR) at the point A (i.e., subsoil top; refer to Figure 2) in a GRPS embankment under static and earthquake conditions. The SAR is the ratio of the vertical stress on the subsoil (σ_{sub}) to overburden stress including surcharge as defined below.

$$\text{SAR} = \frac{\sigma_{sub}}{(\lambda.h+q)} \quad (4)$$

The SAR value lies under 0 to 1, 0 value of the SAR is denoting that all embankment load including surcharge is transferred to the pile top (full mobilisation of soil arching), whereas unit value of SAR implies that no soil arching (i.e., vertical stress on subsoil equal to the overburden stress including surcharge). In Figure 4, it is shown that the SAR decreases up to 0.3 m and 0.5 m embankment height for static and earthquake conditions, respectively. This embankment height denotes the inner arch of soil arching. Further, it increases with an increase of embankment height up to 1.9 m embankment height for both conditions. This embankment height representing to outer arch of soil arching. The SAR again decreases if embankment height extends beyond the outer arch. It is also evident that the SAR is higher at the base of embankment in the earthquake condition compared to the static condition. Thus, an earthquake excitation significantly influenced the soil arching in a GRPS embankment.

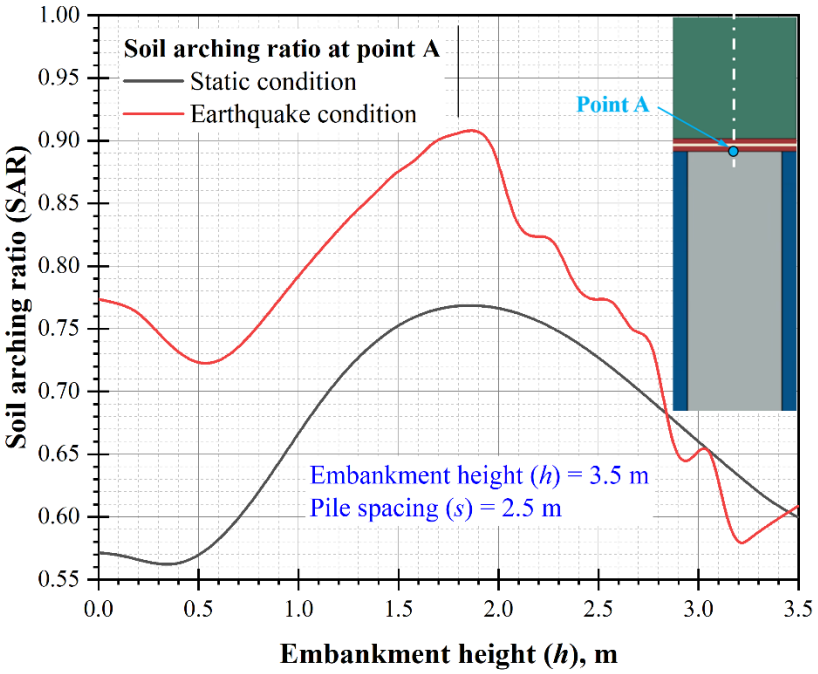

Figure 4. Effect of earthquake on soil arching ratio at point A

Figure 5 shows a comparison of the SAR obtained using different design approaches and the present study. The embankment height (*h*) and pile spacing (*s*) are fixed at 3.5 and 2.5 m, respectively. It is shown that all design approaches and static condition underpredict the SAR compared to earthquake condition as simulated in this study. It may be due to the different shapes of soil arching mobilisation considered in different design approaches and the ignorance of the effect of seismic activities. Therefore, it is crucial to consider seismic excitation in the GRPS embankment design.

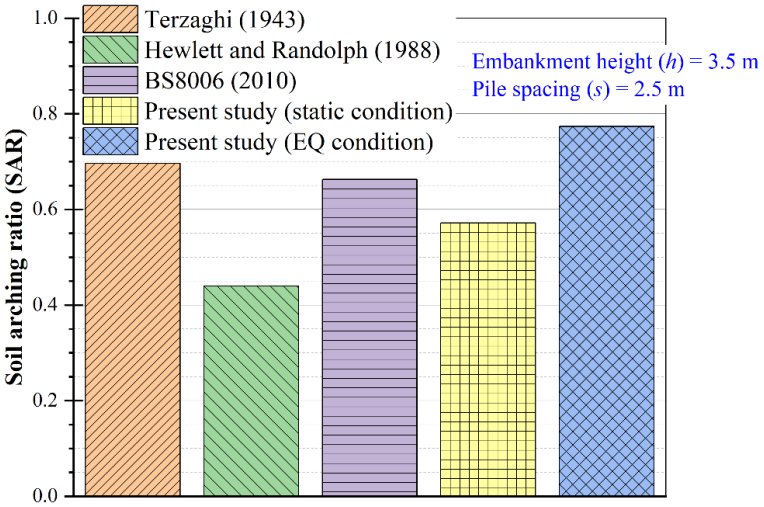

Figure 5. Comparison of SAR with different design approaches

4 Conclusions

In the present study, the soil arching in a GRPS embankment is assessed under the earthquake condition. Based on the results following findings may conclude:

- The soil arching is severely affected under an earthquake excitation. Inclusion of a geosynthetic reinforcement can enhance soil arching even during the earthquake activities. Thus, the use of geosynthetic layers is recommended in the pile-supported embankments irrespective of seismically active or non-active regions.
- The SAR is higher at the base of the embankment in the seismic excitation compared to the static condition which means subsoil experienced a higher stress in the earthquake condition.
- The comparison of SAR with different design approaches reveals that the design approaches of the GRPS embankment need revision to cater for the effects of seismic excitation.

5 References

BS8006-1: (2010) Code of Practice for Strengthened/reinforced Soils and Other Fills. British Standards Institution, ISBN 978-0-580-53842-1.

Daniell, J. E. and Love, D. (2010). The socio-economic impact of historic Australian earthquakes. In Australian Earthquake Engineering Society 2010 Conference, pp 8.

Doyle, N. F. (1980). Railway track design: a review of current practice.

Esveld, C. (2001). Modern railway track (Vol. 385). Zaltbommel: MRT-productions.

Fagundes, D. F., Almeida, M. S., Thorel, L., & Blanc, M. (2017). Load transfer mechanism and deformation of reinforced piled embankments. Geotextiles and Geomembranes, Vol 45, No 2, pp 1-10.

Geoscience Australia. Historic Earthquakes of Australia. Available online: https://geoscience-au.maps.arcgis.com/apps/MapSeries/index.html?appid=72ad590cc9364e41b06907406bb7712e (accessed on 14 September 2021).

Han, G. X. Gong, Q. M. and Zhou, S. H. (2015). Soil arching in a piled embankment under dynamic load. International Journal of Geomechanics, Vol 15, No 6, pp 04014094.

Han, J. and Gabr, M. A. (2002). Numerical analysis of geosynthetic-reinforced and pile-supported earth platforms over soft soil. Journal of geotechnical and geoenvironmental engineering, Vol 128, No 1, pp 44-53.

Hewlett, W. J. and Randolph, M. F. (1988) Analysis of piled embankments. International Journal of Rock Mechanics and Mining Sciences and Geomechanics Abstracts, Vol 25, No 6, pp 297-298.

Huang, J. and Han, J. (2010). Two-dimensional parametric study of geosynthetic-reinforced column-supported embankments by coupled hydraulic and mechanical modeling. Computers and Geotechnics, Vol 37, No 5, pp 638-648.

Iglesia, G. R. Einstein, H. H. and Whitman, R. V. (2014). Investigation of soil arching with centrifuge tests. Journal of Geotechnical and Geoenvironmental engineering, Vol 140, Vo 2, pp 04013005.

Liu, H. L. Ng, C.W. and Fei, K. (2007). Performance of a geogrid-reinforced and pile-supported highway embankment over soft clay: case study. Journal of Geotechnical and Geoenvironmental Engineering, Vol 133, No 12, pp 1483-1493.

Lysmer, J. and Kuhlemeyer, R. L. (1969). Finite dynamic model for infinite media. Journal of the Engineering Mechanics Division, Vol 95, No 4, pp 859-877.

Meena, N. K. Nimbalkar, S. Fatahi, B. and Yang, G. (2020). Effects of soil arching on behavior of pile-supported railway embankment: 2D FEM approach. Computers and Geotechnics, Vol 123, pp 103601.

Meena, N. K. Nimbalkar, S. and Fatahi, B. (2021). Finite Element Analysis of Soil Arching in Piled Embankment. In International Conference of the International Association for Computer Methods and Advances in Geomechanics, pp 817-824. Springer, Cham.

Meena, N. K. and Nimbalkar, S. (2019). Effect of water drawdown and dynamic loads on piled raft: Two-dimensional finite element approach. Infrastructures, Vol 4, No 4, pp 75.

Nimbalkar, S. Indraratna, B. Dash, S. K. and Christie, D. (2012). Improved performance of railway ballast under impact loads using shock mats. Journal of geotechnical and geoenvironmental engineering, Vol 138, No 3, pp 281-294.

Niu, T. Liu, H. Ding, X. and Zheng, C. (2018). Model tests on XCC-piled embankment under dynamic train load of high-speed railways. Earthquake Engineering and Engineering Vibration, Vol 17, No 3, pp 581-594.

Nunez, M. A. Briançon, L. and Dias, D. C. F. S. (2013). Analyses of a pile-supported embankment over soft clay: Full-scale experiment, analytical and numerical approaches. Engineering Geology, Vol 153, pp 53-67.

Pham, H. V. and Dias, D. (2019). 3D numerical modeling of a piled embankment under cyclic loading. International Journal of Geomechanics, Vol 19, No 4, pp 04019010.

Potyondy, J. G. (1961). Skin friction between various soils and construction materials. Geotechnique, Vol 11, No 4, pp 339-353.

Rui, R. Han, J. Van Eekelen, S. J. M. and Wan, Y. (2019). Experimental investigation of soil-arching development in unreinforced and geosynthetic-reinforced pile-supported embankments. Journal of Geotechnical and Geoenvironmental Engineering, Vol 145, No 1, pp 04018103.

Terzaghi, K. (1943). Theoretical soil mechanics. John Wiley & sons. New York, pp 11-15.

Wu, L. Jiang, G. and Ju, N. (2019). Behavior and numerical evaluation of cement-fly ash-gravel pile-supported embankments over completely decomposed granite soils. International Journal of Geomechanics, Vol 19, No 6, pp 04019048.

Zhang, Z. Han, J. and Ye, G. (2014). Numerical investigation on factors for deep-seated slope stability of stone column-supported embankments over soft clay. Engineering Geology, Vol 168, pp 104-113.